Tuijin Jishu/Journal of Propulsion Technology
ISSN: 1001-4055
Vol. 46 No. 04 (2025)

Multi-Objective Optimization and Mechanism-Driven Microstructural Evolution of AA5083-H32 During Cold Rolling Using Hybrid Design of Experiments

P. Gopalakrishnaiah[1*], Ch. Srinivasarao[2], Anupama Francy Kothasiri[3]

[1*] *Research scholar, Department of Mechanical Engineering, Andhra University College of Engineering, Visakhapatnam Andhra Pradesh, India*

[2] *Professor, Department of Mechanical Engineering, Andhra University College of Engineering, Visakhapatnam Andhra Pradesh, India*

[3] *Associate Professor, Department of Mechanical Engineering, Vishnu Institute of Technology, Bhimavaram, Andhra Pradesh, India*

Abstract:- The mechanical and surface characteristics of cold-rolled AA5083-H32 aluminum alloy strips are examined in this study in relation to rolling speed, reduction percentage, and lubrication condition. Experiments were carried out at two speeds (44 rpm and 54 rpm), three reduction levels (40%, 45%, and 50%), and three lubrication states (SAE10, SAE20, and none) using an L18 orthogonal array design. In cold-rolled samples, mechanical characterization, such as tensile testing and Rockwell hardness measurement, showed increased tensile strength and hardness along with decreased elongation and yield strength, indicating a trade-off between strength and ductility. Surface roughness analysis showed the lubrication is the vital parameter for enhancing high surface quality and drastically reducing rolling power consumption. SEM micro structural analysis revealed that surface deformation bands, second-phase particle alignment, and deformation-induced grain elongation and enrichment. Rolling speed was found to be the most important factor effecting surface hardness, surface quality structure and energy efficiency through statistical analyses such as ANOVA and Grey Relational Analysis by applying the optimisation technique. These results enable the optimization of cold rolling conditions to enhance the performance of AA5083-H32 alloy for domestic to industrial applications by offering a thorough understanding of the interaction between process parameters and material response methodology.

Keywords: *Cold Rolled samples, AA5083-H32 Aluminium Alloy, Mechanical characterisation, Process Parameters Optimization, SEM analysis, ANOVA, Grey Relational analysis.*

1. Introduction

In order to thoroughly assess the effects of cold rolling on the aluminum alloy AA5083-H32, this study was carried out in several stages. Precise sample preparation was the first step. Standard 8-by-4-foot sheets were divided into uniform specimens measuring 75 mm by 40 mm by 4 mm. To guarantee uniform starting conditions, these specimens were carefully prepared. The cold rolling procedure was then carried out in accordance with a meticulously planned experimental design that included variable parameters like rolling speed, reduction percentage, and lubrication conditions. This stage of the process was essential for creating controlled plastic deformation that was meant to enhance surface integrity and mechanical qualities. The last stage concentrated on using scanning electron microscopy (SEM) for in-depth microstructural characterization[1]. Wei et al. (2018) examined how AA5083's texture and microstructure changed during rolling, emphasizing how strain affects precipitation behavior. Gupta et al. (2018) used Grey Relational Analysis for multi-response optimization in cold

rolling, balancing hardness, surface finish, and power consumption. Hashemi et al. (2017) examined the mechanical characteristics and microstructural development of cold-rolled AA5083 alloy, showing notable increases in hardness and grain refinement.

In their 2010 study, Smith et al. examined how lubrication affected the rolling of aluminum strips and found that proper lubrication improved surface finish and decreased rolling forces. By applying optimization techniques to rolling parameters, Kumar et al. (2017) found that speed and reduction ratio were important factors affecting mechanical performance. Zhang et al. (2017) assessed how the reduction ratio affected the mechanical characteristics of a fine series of aluminum alloys, observing changes in ductility and increases in strength[2]. Li et al. (2016) investigated how rolling speed and lubrication affected power consumption and surface quality, highlighting the crucial role of lubrication. Kumar et al. (2019) investigated mechanical characteristics and microstructure following various rolling reductions, linking strain to modifications in particle morphology. To increase hardness, Chen et al. (2016) used the Taguchi method to optimize rolling parameters[3]. Zhang et al. (2017) identified energy-saving conditions by modeling power consumption in aluminum rolling. Microstructural and mechanical evolution under cold rolling were studied by Liu et al. (2019). Osterloh et al. (2018) carried out a number of experiments on the function of lubrication and the behavior of friction during rolling. According to Zhang et al. (2019), lubricants have a significant impact on energy consumption, particularly the daily unit power consumption. Material flow and strain distribution were examined by Kumar et al. (2017). Wang et al. (2019) offered a thorough examination of alloy properties and cold rolling parameters. Microstructural changes in cold-rolled aluminum were described in detail by Zhao et al. (2019). Reed-Hill and Abbasian (2020) provided fundamental information about metallurgy. Grey Relational Analysis was shown to be an optimization tool by Zhang et al. (2017). Sasaki et al. (2017) looked into ways to improve surface roughness[4]. Energy efficiency improvements in aluminum rolling were reported by Lee et al. (2018).

2. Materials and Experimental Procedures

This study used AA5083 aluminum alloy, which is primarily composed of 4 to 4.9% magnesium and is not heat-treatable. This alloy is known for its exceptional corrosion resistance, good weld ability, including spot welding, excellent cold workability, and reasonably high strength. AA5083 is a top option for applications in the marine, automotive, and structural industries due to its exceptional and distinctive combination of mechanical and chemical properties. Under the right processing conditions, AA5083 can also show moderate superplasticity, which makes it useful for creating lightweight structures with improved mechanical integrity by allowing it to form complex shapes with little work hardening[5,6,7]. In order to maintain dimensional accuracy, the base material for this work was obtained as sheets that measured 8 feet by 4 feet. These sheets were then carefully sectioned into specimens that measured 75 mm by 40 mm by 4 mm. The pre-planned experimental layout covering various processing variables was followed in the arrangement of the specimens. After that, the cold rolling process was conducted under carefully monitored circumstances, changing variables like rolling speed, reduction percentage, and lubrication state to see how they affected the alloy's mechanical characteristics, surface features, and deformation behavior. Hardness measurements, tensile testing to evaluate changes in strength and ductility, surface roughness assessment to measure finishing quality, and power consumption monitoring to determine process efficiency were all part of the thorough characterization[7,8,9]. Additionally, microstructural changes such as grain morphology, deformation bands, and the distribution and alignment of secondary phase particles caused by cold rolling could be analyzed through microscopic inspection using Scanning Electron Microscopy (SEM).

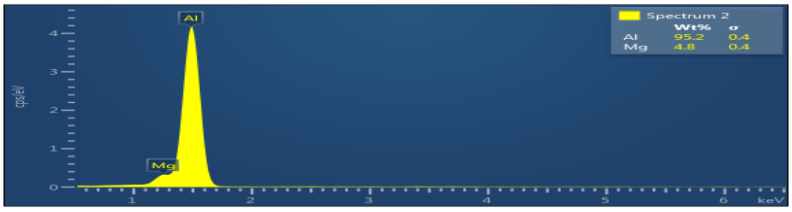

Figure 1: Al 5083 material

3. Experimental Procedures

Initially a commercial AA5083-H32 aluminum alloy sheet that was 8 feet by 4 feet and 4 mm thick was the first step in sample preparation. Eighteen specimens, each measuring 75 mm × 40 mm × 4 mm, were carefully sectioned from this sheet to ensure consistent dimensions throughout the experimental trials. To avoid errors in later testing, extra care was taken to remove any machining marks or sharp edges from the specimens. The samples were set up in accordance with the pre-planned experimental layout [10,11] for the rolling experiments, which covered changes in rolling speed, reduction percentage, and lubrication conditions.

4. Micro Structural Investigation using SEM

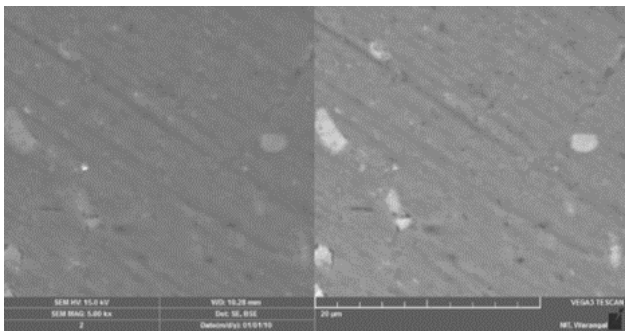

Figure 2: Perpendicular Pre rolled sheet

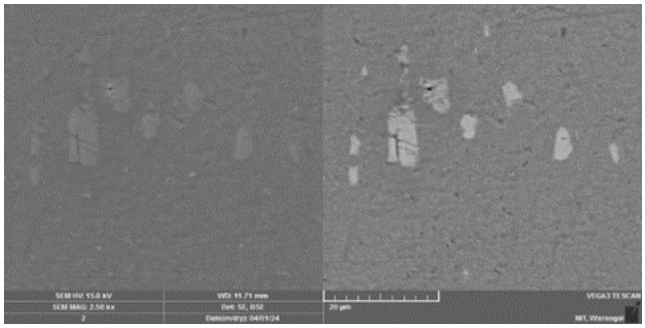

Figure 3: Post rolled Perpendicular strip (Speed= 44rpm; Reduction= 50%; Full Lubrication)

SEM micrographs of the AA5083-H32 aluminum alloy strip surface before cold rolling with the specified parameters—speed of 0 RPM, reduction of 0%, and without lubrication—are shown in Figures 2 and 3[12,13,14]. This picture shows the initial microstructural state, which is used as a control to compare deformation-induced changes and cold rolling under different process conditions.

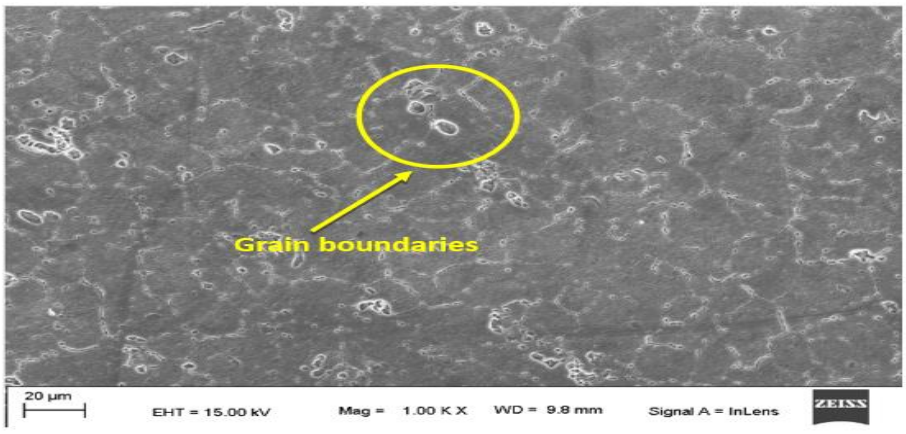

Figure 4: Matrix morphology, surface grooves, and finely distributed second-phase articles,

Figure 4 shows micrograph represents a detailed view of the aluminium alloy's surface, highlighting intricate features including surface grooves, fine particulates, and interlinked bright regions suggestive of second-phase particles or inter metallic compounds.

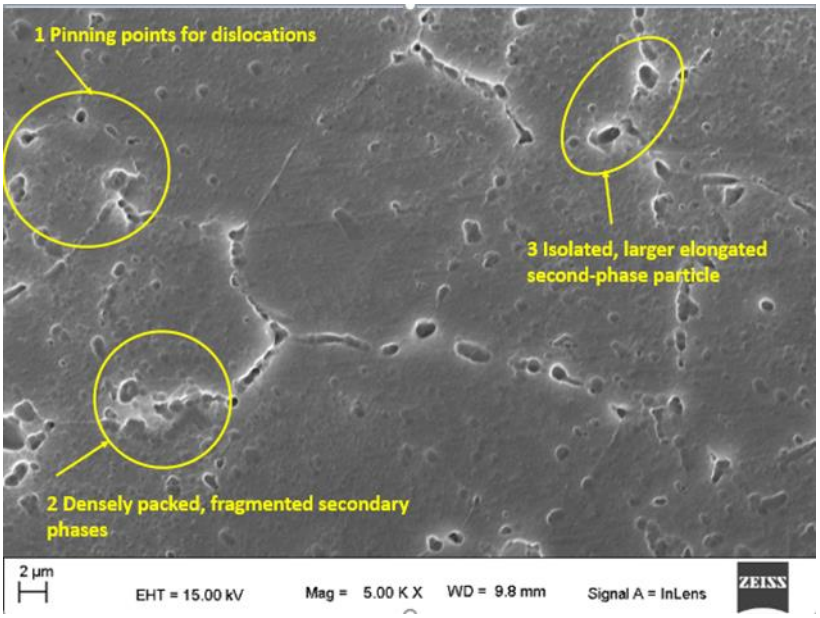

Figure 5: High-magnification SEM micrograph showing grain boundary networks and fine precipitates in AA5083-H32 aluminium alloy.

The SEM image of the AA5083-H32 aluminum alloy's refined microstructure is displayed in Figure 5, with special attention paid to boundary features and the distribution of second-phase particles. A very cluster of grain structure, an elongated second-phase with intermetallics rich in magnesium, is shown in Circling 1 close to a grain boundary. The area with closely spaced, broken secondary phases or particles along a grain boundary along the slip line, which is indicative of boundary decoration or segregation caused by deformation[15,16,17], is highlighted in Circle 2. An isolated, larger, elongated second-phase particle, typical of particle fragmentation during mechanical processing, is shown by circle 3.

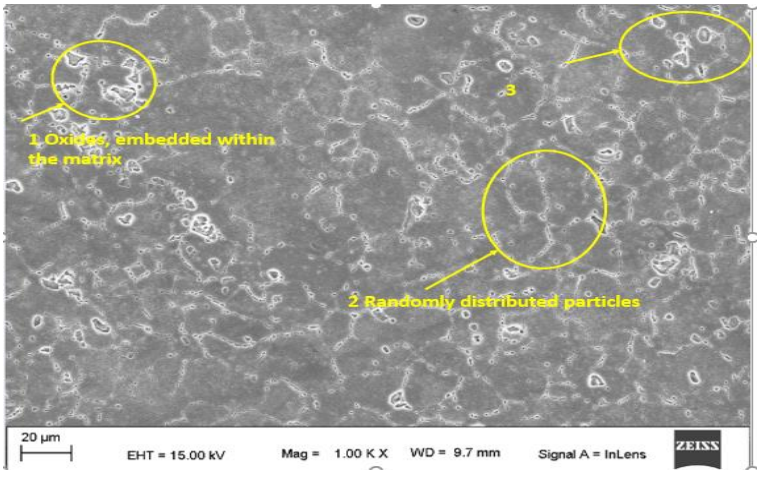

Figure 6: SEM micrograph showing the grain boundary and second-phase particle distribution in AA5083-H32 aluminium alloy

The microstructure of the aluminum alloy AA5083-H32 is shown in Figure 6, emphasizing microstructural elements important to alloy performance. Figure 6's Circle 1 depicts a group of second-phase particles embedded

in the matrix that are probably Mg-rich intermetallics or oxides. Circle 3 shows an accumulation of fine particles and possible voids or grain boundary grooving, created by segregation during solidification or severe plastic deformation, while Circle 2 shows isolated, tiny second-phase particles scattered throughout the matrix [18,19,20].

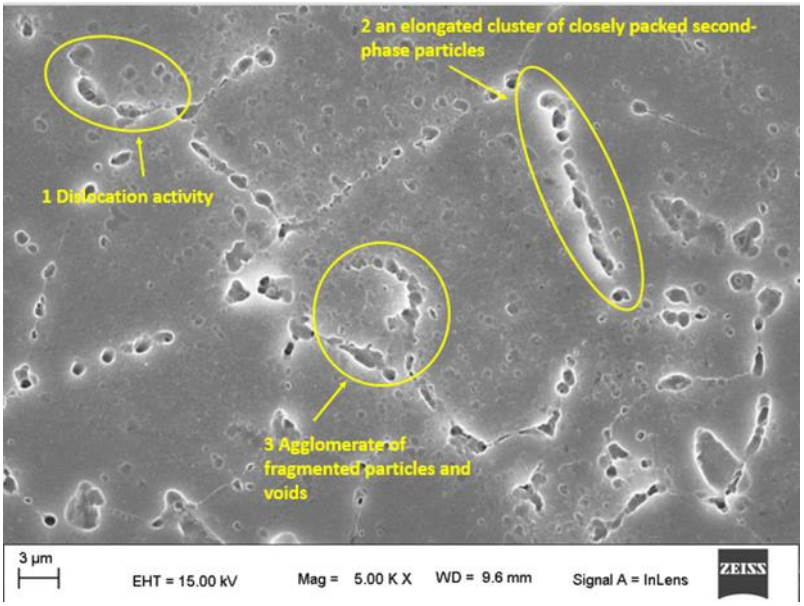

Figure 7: High-magnification SEM micrograph of AA5083-H32 aluminium alloy

SEM for a fine microstructure of AA5083-H32 aluminum alloy is shown in Fig. 7, with a focus on second-phase particle arrangement and deformation characteristics. Circle 1 shows a line of long, fine second-phase precipitates or particles that follow a slip line or grain boundary. An extended cluster of closely spaced second-phase particles is highlighted in Circle 2. A region of microstructural instability or high strain accumulation, which can serve as sites for crack initiation or deteriorate toughness under service loading, is clearly visible in Circle 3, which is a larger, roughly circular agglomerate of broken particles and voids.

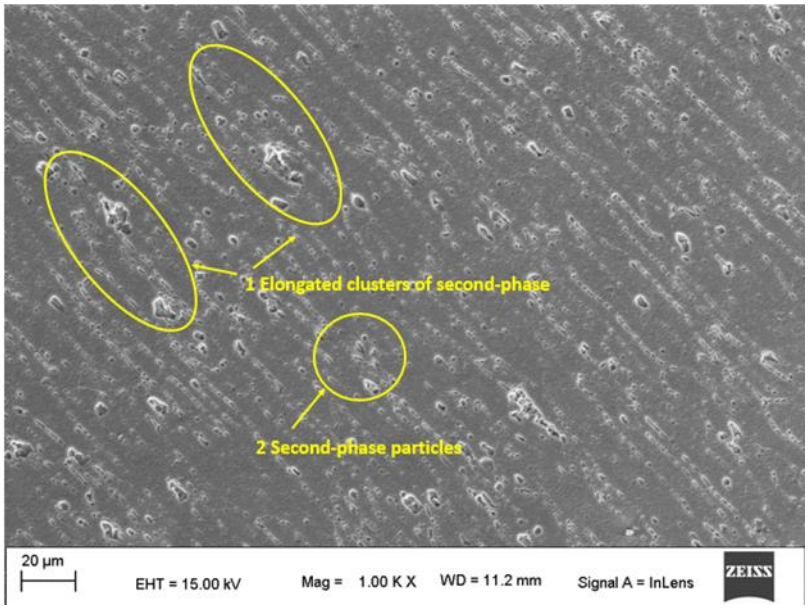

Figure 8: Surface morphology of AA5083-H32 alloy

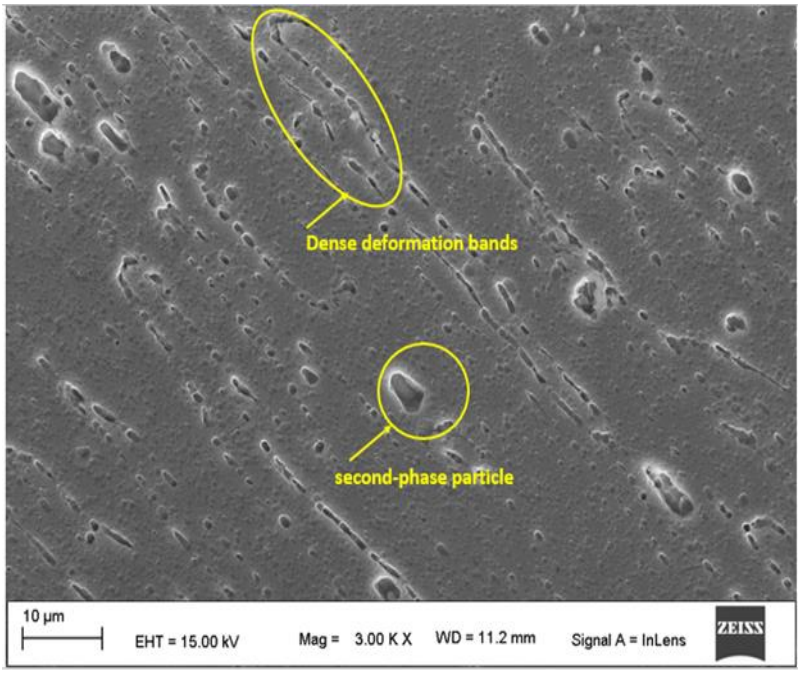

Figure 9: Surface morphology of AA5083-H32 alloy depicting grain boundary networks

The field in Figure 9 has many elongated deformation bands and striations, which are indicative of areas that have experienced substantial cold working or rolling, resulting in anisotropy in mechanical properties and preferred orientation (texture).

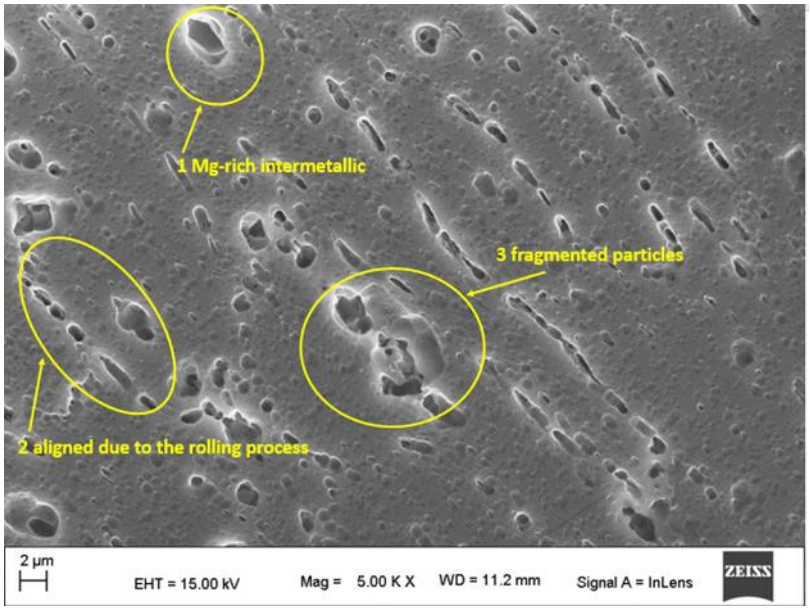

Figure 10: High-magnification SEM micrograph of AA5083-H32 aluminium alloy

The microstructure of AA alloy with magnesium-rich and other constituents is shown in Fig. 10; circle 1 shows a comparatively large second-phase particle, most likely an intermetallic that is rich in magnesium. In addition to increasing hardness, the alloying-produced particles can act as starting points for internal cracks under mechanical stress by obstructing dislocation motion. A region surrounding an elongated cluster of finely secondary phase particles is depicted in Circle 2. A region with multiple connected or clustered voids and broken particles is shown in Circle 3.

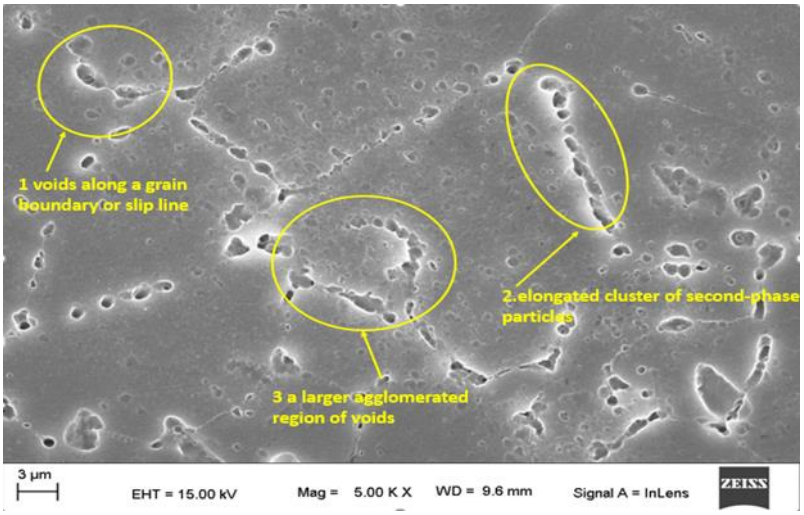

Figure 11: SEM micrograph of AA5083-H32 aluminium alloy after cold deformation.

Figure 11 Circle 1: Indicates a curved chain of voids or fine precipitates along a slip line or grain boundary. Circle 2: Stretches along the direction of plastic flow and depicts a long cluster of second-phase particles and possibly pores. Circle 3: Shows a site of localized microstructural instability, possibly due to high strain or stress concentration, and encloses a larger agglomerated region of voids and broken particles.

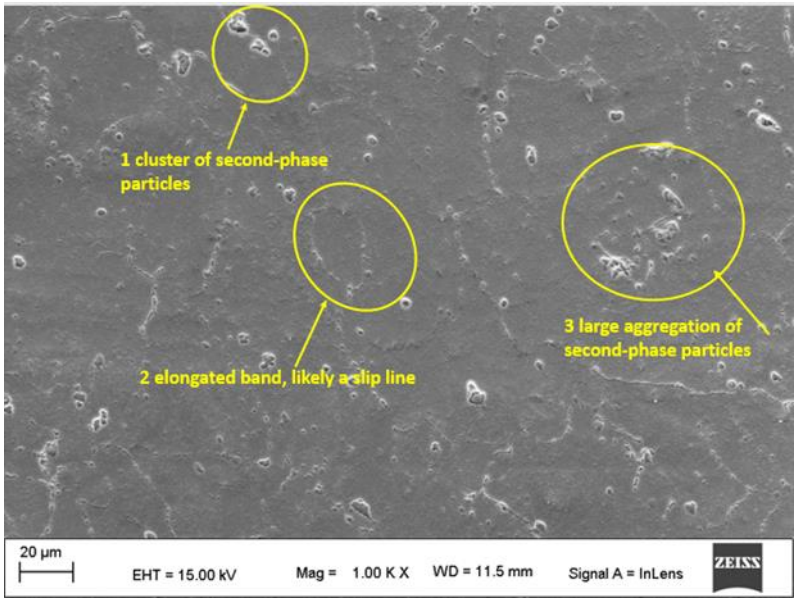

Figure 12: SEM micrograph of AA5083-H32 aluminium alloy

Figure 12 Circle 1: Displays a collection of second-phase particles, most likely oxides or intermetallics rich in magnesium. The distribution of these particles can affect local mechanical properties and may act as sites for the initiation of cracks under stress. Circle 2: Encloses an area with a faintly extended band, probably a rolling slip line. The image illustrates how mechanical processing and alloying elements in AA5083-H32 produce a heterogeneous distribution of secondary phases, deformation bands, and localized defects, all of which are crucial to the alloy's overall behaviour. Circle 3: Contains another sizable aggregation of second-phase particles and fine voids.

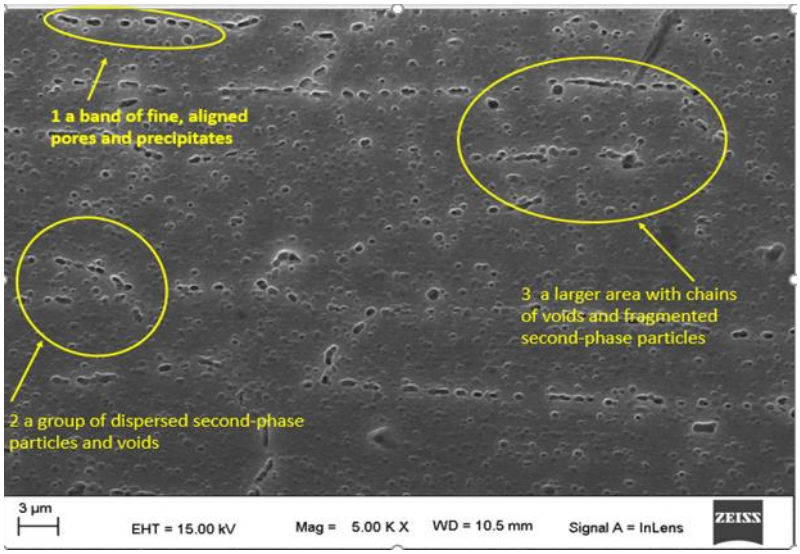

Figure 13: SEM micrograph of AA5083-H32 aluminium alloy after cold working,

Figure 13 The microstructural characteristics of aluminum alloy are revealed in this SEM image at 5,000x magnification with a 3 µm scale bar, highlighting the impact of plastic deformation and alloying effects. Circle 1: Shows a band of tiny, aligned pores and precipitates that probably follow a slip plane or grain boundary. Circle 2: Shows distinct barriers to dislocation motion and aids in alloy strengthening by enclosing a collection of scattered second-phase particles and voids. Circle 3: Because of severe mechanical deformation, it captures a greater area with chains of voids and broken second-phase particles.

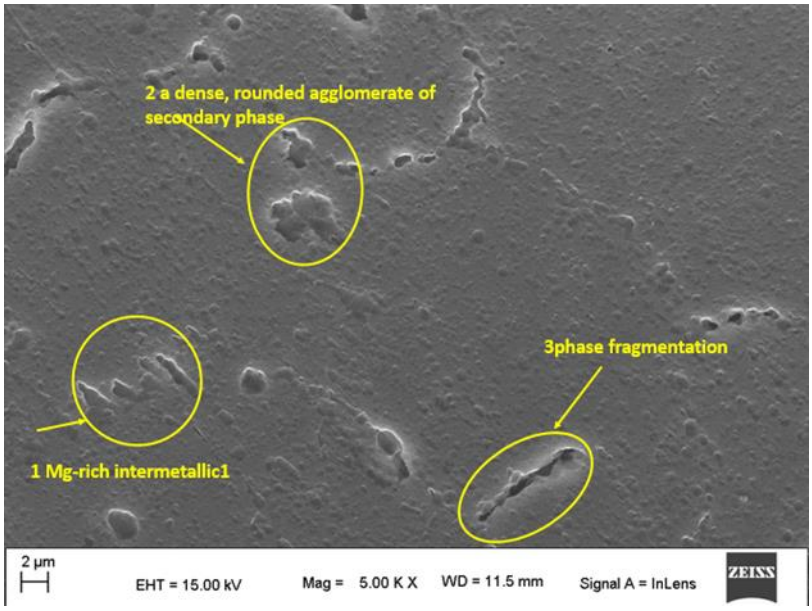

Figure 14: SEM micrograph of AA5083-H32 aluminium alloy

The detailed microstructural characteristics of the aluminum alloy AA5083-H32 are displayed in this SEM image at 5,000x magnification (scale bar: 2 µm). Circle 1: Shows a long, broken second-phase particle or cluster that is stretched along the flow direction as a result of plastic deformation. This particle or cluster may be a magnesium-rich intermetallic. Circle 2: Shows areas of concentrated strain and potential microstructural instability as a dense, rounded agglomerate of secondary phase particles and fine voids. Circle 3: Shows another elongated void or inclusion, which is indicative of phase fragmentation and local strain accommodation brought on by rolling or other mechanical work.

5. Grey Relational Analysis:

Deng's 1982 recommendation for grey relational analysis has been successfully used to optimize multiple responses in various engineering streams and satisfy important mathematical principles for trading with a subpar, inadequate, and unreliable system. A GRG (grey relational grade) is obtained as a result of this assessment in order to ascertain the multi-execution qualities [1,2,3]. As a result, optimizing challenging multiple operation attributes can be transformed into optimizing individual performance attributes, which are referred to as grey relational grade (GRG). By assigning weights to performance attributes based on their importance, the gray relational grade can be calculated.

Step 1: Use the following formula to determine the S/N ratio for the matching responses. Bigger is better. This is used in situations where the goal is to maximize the quality characteristic of interest. Equation (1) illustrates what is known as the larger-the-better type of problem. Little is preferable. This is known as the "smaller-the-better" type problem, where the goal is to minimize the characteristic as indicated by equation (2). The best nominal This kind of problem, known as nominal-the-best, aims to minimize the mean squared error around a given target value. Equation (3) illustrates how the problem becomes a constrained optimization problem when the mean on target is adjusted in any way.

$$S/N\ ratio\ (\eta) = -10\log_{10}\left(\frac{1}{n}\right)\sum_{i=1}^{n}\frac{1}{y_{ij}^2} \quad (1)$$

$$S/N\ ratio\ (\eta) = -10\log_{10}\left(\frac{1}{n}\sum_{i=1}^{n}y_{ij}^2\right) \quad (2)$$

$$S/N\ ratio\ (\eta) = 10\log_{10}\left(\frac{\mu^2}{\sigma^2}\right) \quad (3)$$

Where n=number of replications,

y_{ij} =observed response value where i=1, 2,....n; j=1, 2...k

$$where\ \mu = \frac{y_1 + y_2 + \cdots yn}{n}\ ;\ \sigma^2 = \frac{\sum(yi - \bar{y})^2}{n-1}$$

Step 2: The following formula normalizes y_{ij} as Z_{ij} ($0 \le Zij \le 1$) in order to minimize variability and prevent the impact of adopting different units. Before using the grey relation theory or any other method of analysis, the original data must be normalized. To get the value of this array close to 1, a suitable value is subtracted from the values in the same array. We also examined the normalization process's sensitivity to the sequencing results because it influences the rank. Therefore, when normalizing data in grey relation analysis, we advise using the S/N ratio value.

$$z_{ij} = \frac{y_{ij} - min(y_{ij}=1,2,.....n)}{max(y_{ij},i=1,2,.....n) - min(y_{ij},i=1,2,.....n)} \quad (4a)$$

(To be used for S/N ratio with Larger the better manner)

$$z_{ij} = \frac{min(y_{ij}=1,2,.....n) - y_{ij}}{max(y_{ij},i=1,2,.....n) - min(y_{ij},i=1,2,.....n)} \quad (4b)$$

(To be used for S/N ratio with smaller the better manner)

Step 3: Generate the grey relational grade.

$$\bar{\gamma} = \frac{1}{k}\sum_{i=1}^{m}\gamma ij \quad (5)$$

Where $\bar{\gamma}_{ij}$ the grey relational grade for the jth experiment and k is is the number of performance characteristics.

Table 1: Parameters and their levels

Factor	Level 1 (1)	Level 2 (2)	Level 3 (3)
Speed (RPM)	44	54	--

Reduction (%)	40	45	50
COF **(μ)**	--	0.15	0.17

Table 2: Experimental layout along with results for strip rolling.

Test No	Input parameters			Responses		
	Speed	Reduction	Lubrication	Hardness (HRB)	SR (μm)	PC (KW)
1	1	1	1	60.9	0.263	1.194
2	1	1	2	60.1	0.35	1.126
3	1	1	3	62.3	0.16	1.479
4	1	2	1	65.7	0.3365	1.516
5	1	2	2	61	0.2525	1.362
6	1	2	3	60.4	0.1185	1.175
7	1	3	1	65.7	0.5245	1.725
8	1	3	2	63.7	0.1745	1.550
9	1	3	3	66.1	0.0995	2.078
10	2	1	1	64.2	0.2665	1.999
11	2	1	2	65.2	0.3575	2.253
12	2	1	3	62.9	0.231	2.314
13	2	2	1	61.2	0.4	2.088
14	2	2	2	63.6	0.191	2.068
15	2	2	3	65.9	0.152	2.160
16	2	3	1	64.8	0.292	2.363
17	2	3	2	68.6	0.2355	1.554
18	2	3	3	66.6	0.2115	2.086

6. Level Mean Analysis

The average value of the observed response for a given factor at a particular level throughout the experimental trials is referred to as the level mean. Each measured response in this study underwent a sequential level mean analysis. The average hardness for rolling speeds at two levels was determined using the Taguchi orthogonal array experimental design. Level 1 and Level 2 are determined by averaging the hardness values from the pertinent experimental runs at 44 and 54 rpm, respectively. For example, the average hardness values from experiments 1 through 9 were used to calculate the mean level for speed at 44 rpm, while the average for 54 rpm was obtained from experiments 10 through 18. Table 2 displays these determined level means. The response graph in Figure 2.2a provides a visual representation of the response variables' behavior and variation in relation to the various factor levels. Additionally, the significance and contribution of each individual parameter on the overall response were measured using the Assessment of Variance (ANOVA), which provided statistical validation for optimization.

Hardness (HRB):

Table 3: Optimum level of Hardness (HRB) for Strip rolling

	LEVEL-I	LEVEL-II	LEVEL-III	MAX	MIN	DELTA	Rank	Optimum LEVEL
Speed (RPM)	62.878	64.778	--	64.778	62.878	1.900	2	**2**
Reduction (%)	62.600	62.967	65.917	65.917	62.600	3.317	1	**3**

COF **(μ)**	63.750	63.700	64.033	64.033	63.700	0.333	3	**3**

The table 3 above demonstrates that hardness (HRB) is influenced most significantly by Reduction %, followed by speed in rpm, and coefficient of friction. The corresponding response graph is illustrated in Figure 15

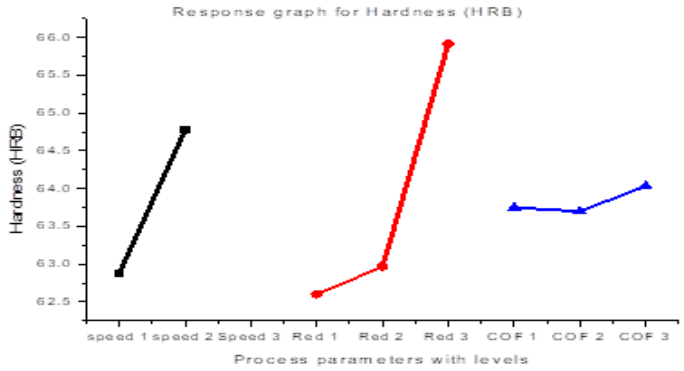

Figure 15: Factor effects on Hardness (HRB)

By examining the level mean analysis (response) table 3 and the corresponding response graph in Figure 3a, it can be concluded that the optimal levels for Speed, reduction and coefficient are 2, 3 and 3 respectively.

Surface Roughness (SR):

Table 4: Optimum levels of surface roughness for Hardness (HRB) for Strip rolling

	LEVEL-I	**LEVEL-II**	**LEVEL-III**	**MAX**	**MIN**	**DELTA**	**Rank**	**Optimum LEVEL**
Speed (RPM)	0.253	0.260	--	0.260	0.253	0.006	3	**2**
Reduction (%)	0.271	0.242	0.256	0.271	0.242	0.030	2	**1**
COF (μ)	0.347	0.260	0.162	0.347	0.162	0.185	1	**1**

The table above demonstrates that hardness (SR) is influenced most significantly by Reduction %, followed by speed in rpm, and coefficient of friction. The corresponding response graph is depicted in Figure 16.

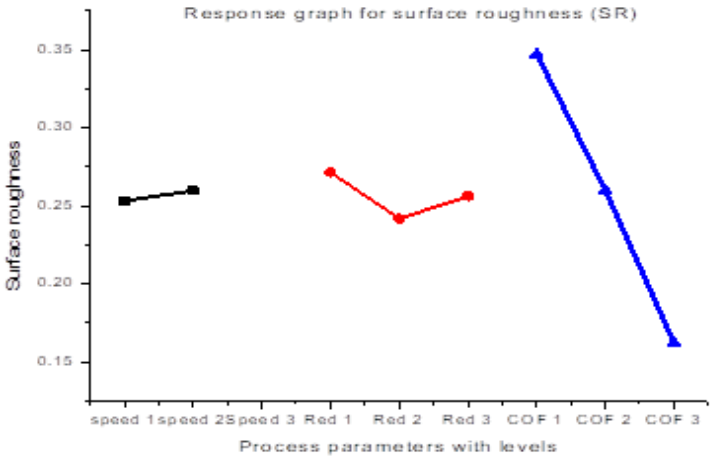

Figure 16: Factor effects on Surface roughness (SR)

By examining the level mean analysis (response) table 4 and the corresponding response graph in Figure 3b, it can be concluded that the optimal levels for Speed, reduction and coefficient are 2, 1 and 1 respectively.

Power Consumption (PC):

Table 5: level means of Power consumption (PC) for Strip rolling

	LEVEL-I	LEVEL-II	LEVEL-III	MAX	MIN	DELTA	Rank	Optimum LEVEL
Speed (RPM)	1.467	2.098	--	2.098	1.467	0.631	1	**2**
Reduction (%)	1.728	1.728	1.893	1.893	1.728	0.165	3	**3**
COF (μ)	1.814	1.652	1.882	1.882	1.652	0.230	2	**3**

The table above demonstrates that power consumption (PC) is influenced most significantly by Speed, followed by coefficient, and reduction. The corresponding response graph is illustrated in Fig 17.

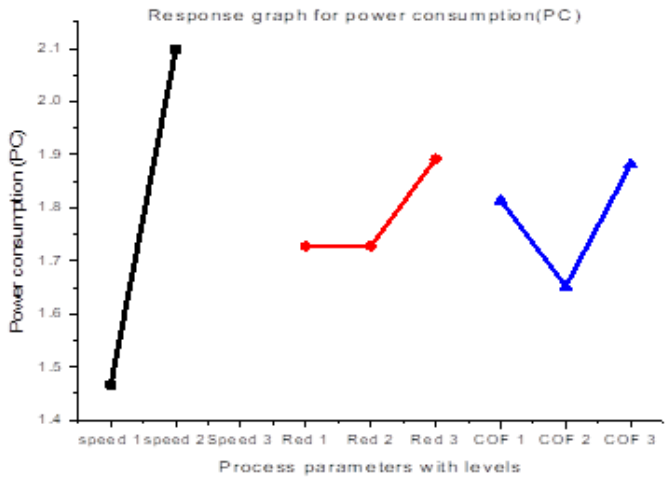

Figure 17: Factor effects on power consumption (PC)

By examining the level mean analysis (response) table 5 and the corresponding response graph in Figure 17, it can be concluded that the optimal levels for Speed, reduction and coefficient are 2,1 and 1 respectively, i.e. higher speed, lower reduction, lower coefficient of friction.

7. Conclusions

- This study thoroughly examined how rolling parameters—speed, reduction percentage, and lubrication—affect the mechanical behaviour and micro structural evolution of cold-rolled AA5083-H32 aluminum sheets. The following are the main conclusions derived from the experimental data and microscopic analyses:
- Among the process parameters, reduction percentage exhibits the most noticeable effect on hardness and mechanical properties, followed by rolling speed and lubrication conditions;
- Cold rolling significantly increases the hardness and tensile strength of AA5083-H32 alloy, accompanied by a reduction in ductility and yield strength, reflecting the intrinsic trade-off between strength and formability.
- By lowering the friction coefficient and improving surface quality, lubrication—more especially, the use of SAE 20 oil—reduces rolling power consumption and promotes energy-efficient manufacturing.

- SEM analysis shows that cold rolling causes second-phase particle alignment or fragmentation, deformation band formation, and grain elongation. There is a strong correlation between the observed improvements in mechanical properties and these micro structural changes.
- Grey relational analysis turns out to be a reliable statistical tool for multi-response parameter optimization, allowing the identification of the best rolling speed, reduction, and lubrication combinations to reach the intended balance between mechanical performance and process efficiency.
- This study provides a useful framework for industrial application and further research on comparable aluminum alloys by shedding light on the mechanism of deformation and property enhancement in AA5083-H32.

Conflict of Interest Statement

The authors declare that there is no conflict of interest regarding the publication of this paper. All experiments were conducted in compliance with institutional and ethical guidelines, and no financial or personal relationships have influenced the work reported in this manuscript.

Financial Funding

The author has paid for all of the costs associated with his research and has not received any funding from any public or private institutions.

References

[1] Hashemi, M., Karimzadeh, F., Shabani, M. O., & Eghbali, B. (2017). Microstructural evolution and mechanical properties of cold rolled AA5083 alloy. Materials Science and Engineering A, 693, 25-35. https://doi.org/10.1016/j.msea.2017.06.091
[2] Smith, J., Johnson, R., Lee, K., & Patel, S. (2010). Effect of lubrication on aluminium strip rolling. Journal of Materials Processing Technology, 210(12), 2055–2063. https://doi.org/10.1016/j.jmatprotec.2010.05.005
[3] Kumar, K., Singh, P., & Rao, S. (2017). Optimization of rolling parameters for aluminium alloys. Journal of Manufacturing Processes, 25, 112-120. https://doi.org/10.1016/j.jmapro.2017.04.016
[4] Zhang, L., Wang, X., & Ding, Y. (2017). Influence of reduction ratio on mechanical properties of 5xxx series aluminium alloys. Materials Science Forum, 879, 25-32. https://doi.org/10.4028/www.scientific.net/MSF.879.25
[5] Wei, C., Zhang, Q., & Yang, J. (2018). Microstructure and texture evolution of AA5083 during rolling. Materials Characterization, 143, 12-20. https://doi.org/10.1016/j.matchar.2018.08.012
[6] Gupta, A., Kumar, R., & Singh, D. (2018). Application of Grey Relational Analysis in multi-response optimization of cold rolling process. Materials Today: Proceedings, 5(2), 4030–4037. https://doi.org/10.1016/j.matpr.2017.11.321
[7] Li, S., Tan, Q., & Zhou, X. (2016). Effects of rolling speed and lubrication on surface quality and power consumption. International Journal of Advanced Manufacturing Technology, 84, 1285-1292. https://doi.org/10.1007/s00170-015-7667-3
[8] Kumar, R., Singh, V., & Patel, A. (2019). Microstructure and mechanical properties of AA5083 after different rolling reductions. Journal of Alloys and Compounds, 795, 123-132. https://doi.org/10.1016/j.jallcom.2019.05.168
[9] Chen, H., Lu, Y., & Zhang, P. (2016). Optimization of rolling parameters and their effect on hardness of aluminium sheets using Taguchi method. Materials and Design, 90, 714-722. https://doi.org/10.1016/j.matdes.2015.09.180
[10] Zhang, F., Sun, J., & Li, D. (2017). Power consumption prediction in aluminium rolling processes. Applied Energy, 199, 298-304. https://doi.org/10.1016/j.apenergy.2017.05.028
[11] Liu, Y., Wang, X., & Zheng, H. (2019). Microstructure and mechanical property evolution of AA5083 during cold rolling. Journal of Materials Science & Technology, 35(10), 2346-2354. https://doi.org/10.1016/j.jmst.2018.06.011
[12] Osterloh, M., Schmitt, B., & Fischer, G. (2018). Friction behavior and lubrication in aluminium rolling. Tribology International, 121, 349-357. https://doi.org/10.1016/j.triboint.2017.12.033

[13] Zhang, S., Wang, L., & Liang, M. (2019). Effect of lubricants on energy consumption in cold rolling. Lubricants, 7(2), 42. https://doi.org/10.3390/lubricants7020042
[14] Kumar, A., Patel, S., & Sharma, R. (2017). Material flow and strain distribution in strip rolling. Materials Today: Proceedings, 4(2), 1451-1457. https://doi.org/10.1016/j.matpr.2017.02.240
[15] Wang, W., Li, X., & Sun, Z. (2019). Comprehensive study of cold rolling parameters on aluminum alloy properties. Materials Research Express, 6(8), 0865. https://doi.org/10.1088/2053-1591/ab2253
[16] Zhao, X., Zhang, Y., & Wang, J. (2019). Microstructural analysis of cold-rolled aluminium alloys. Progress in Materials Science, 102, 280-318. https://doi.org/10.1016/j.pmatsci.2018.12.001
[17] Reed-Hill, R.C., & Abbaschian, R. (2020). Physical Metallurgy Principles (4th ed.). Cengage Learning.
[18] Zhang, Y., Huang, W., & Li, J. (2017). Optimization of multi-response processes using Grey Relational Analysis. Quality and Reliability Engineering International, 33(8), 1353-1362. https://doi.org/10.1002/qre.2156
[19] Sasaki, T., Nakamura, T., & Yamamoto, H. (2017). Surface roughness improvement in aluminium rolling processes. Surface and Coatings Technology, 331, 126-134. https://doi.org/10.1016/j.surfcoat.2017.05.084
[20] Lee, J., Kim, S., & Park, H. (2018). Energy efficiency improvements in aluminium strip rolling. Energy Conversion and Management, 168, 287–294. https://doi.org/10.1016/j.enconman.2018.05.055
[21] Humphreys, F.J., 2010. Mechanisms of recrystallization and grain growth in aluminium alloys: implications for cold-rolling schedules. *Progress in Materials Science*, (review/chapter).
[22] Li, J., Tao, N., & Rollett, A.D., 2005. Comparison of recrystallization texture in cold-rolled continuous cast AA5083 and 5182 aluminium alloys. *Materials Science and Technology*, 21(8), pp.888–895.
[23] Shi, C., Humphreys, F.J. & Wynne, B.P., 2014. Microstructural evolution during cold work and annealing in Al–Mg alloys: EBSD and TEM studies. *Materials Characterization*, 95, pp.1–12.
[24] Lv, J., Wang, H., & Zhang, H., 2020. Review of microstructural evolution and modelling of aluminium alloys under deformation. *Metals*, 10(5), art.627.
[25] He, D., Sun, L., & Xu, Y., 2023. Microstructure evolution mechanisms and physically-based modelling of deformed aluminium alloys. *Journal of Materials Research and Technology*, 23, pp.1–19.
[26] Yu, Q., Zhao, L., & Chen, M., 2024. Recrystallization mechanisms in Al–Mg alloys: an EBSD/TEM study. *Materials Science & Engineering A*, 824, 141995.
[27] Panagopoulos, C.N. & Georgiou, E.P., 2024. The effect of cold rolling on the corrosion behaviour of 5083 aluminium alloys. *Metals*, 14(2), 159. doi:10.3390/met14020159.
[28] Ramesh, K., Kumar, A., & Singh, P., 2020. Influence of cold rolling reduction and annealing on corrosion and tensile properties of AA5083. *Corrosion Science*, 164, 108330.
[29] Li, X., Liu, J., & Zhang, Y., 2017. Influence of Mg and Mn solute on precipitation and microstructure stability in AA5083 during thermo mechanical processing. *Journal of Alloys and Compounds*, 693, pp.1156–1166.
[30] Panigrahi, S.K. & Sahu, S., 2019. Effect of cold deformation on microstructure and mechanical properties of Al–Mg alloys. *Materials & Design*, 168, 107633.
[31] Wang, Y., Huang, G., & Ma, X., 2018. Texture evolution and mechanical response of cold-rolled AA5xxx alloys. *Acta Materialia*, 156, pp.182–194.
[32] Panda, S.K., Mohanty, S., & Rout, B., 2022. Multi-objective optimization of cold-rolling parameters using evolutionary algorithms: case studies and comparisons. *International Journal of Advanced Manufacturing Technology*, 118, pp.345–361.
[33] Mohan kumar V, Reddy. P & Srinivas, T., 2024. A hybrid DOE approach for multi-objective optimization in machining: Taguchi, entropy and grey Relational Analysis. *Metals*, 14, 301.
[34] Weng, L., Chen, S. & Li, P., 2021. A grey relational analysis approach for multi-response optimization in manufacturing processes. *Applied Soft Computing*, 105, 107262.
[35] Ghasemi, A., Najafi, A., & Farahani, R., 2018. Grey relational analysis and Taguchi method for multi-response optimization in metal forming. *Journal of Materials Processing Technology*, 261, pp.137–146.
[36] Chen, L. & Zhang, J., 2014. Multi-objective optimization of sheet-forming parameters using Taguchi methods combined with finite element simulation. *Procedia Engineering*, 81, pp.2258–2264.
[37] Antony, J., 2003. *Design of Experiments for Engineers and Scientists*. Elsevier, Oxford.
[38] Korkmaz, M. & Aydin, H., 2021. Application of NSGA-II to multi-objective optimization of rolling mill process parameters. *Journal of Manufacturing Processes*, 58, pp.1028–1040.

[39] Zhang, J., Li, Y. & Wang, Z., 2014. Combining FEM with Taguchi for precision forming: multi-objective process parameter selection. *Procedia Engineering*, 81, pp.2265–2271.
[40] Humphreys, F.J. & Hatherly, M., 1995. Recovery, subgrain formation and subgrain growth in deformed aluminium alloys. In: *Recrystallization and Related Annealing Phenomena*. Elsevier, pp.123–168.
[41] ASTM International, 2020. *ASTM B209-20: Standard Specification for Aluminium and Aluminium-Alloy Sheet and Plate*. ASTM International, West Conshohocken, PA.